Vitreous and glass-ceramics materials in the SiO_2-Al_2O_3-MeO-M_2O type system

S. PETRESCU, M. MALKI[a,b], M. CONSTANTINESCU, E. M. ANGHEL[*], I. ATKINSON, R. STATE, M. ZAHARESCU

Institute of Physical Chemistry "Ilie Murgulescu" of Romanian Academy, Spl. Independentei 202, 77208, Bucharest, Romania

[a]*CNRS/CEMHTI-1D Av. de la Recherche Scientifique, 45701 Orléans cedex 2, France*

[b]*Polytech' Orléans, Université d'Orléans, 8 rue Léonard de Vinci, 45072 Orléans cedex 2, France*

Several glasses in the SiO_2-Al_2O_3-MeO-M_2O system (where M stands for Na, K while Me represents Mg, Ca, Ba) were prepared by quenching method and their crystallization mechanism and microstructure evolution were investigated by DSC, X-ray diffraction (XRD), Raman spectroscopy and SEM. Multi-component fitting of the asymmetric and split DSC exotherms of crystallization was performed in order to establish crystallization behavior and the thermal stability as differences of the onset of the crystallization temperature (T_{on}) and the glass transition (T_g) for the investigated glasses. Their microstructure was correlated with the electrical conductivity measurements in solid phase. For instance electrical conductivity of three soda alkaline earth aluminosilicate glasses, called 20(Mg/Ca/Ba) glasses, with the same Na_2O/SiO_2 ratio increases in the succession 20Mg> 20Ba> 20Ca as the fraction of the non-bridging oxygen, f_{NBO}, and their more depolymerized silicate species, Q^1 and Q^2.

(Received July 9, 2012; accepted July 19, 2012)

Keywords: Glass, glass-ceramic, Differential Scanning Calorimetry (DSC), Raman spectroscopy, Microstructure, Electrical conductivity

1. Introduction

The MeO-Al_2O_3-SiO_2 glasses are not only the most important type of materials studied by the earth science but also engineered with a wide range of properties (high electrical resistivity, good chemical stability, excellent optical and mechanical properties, moderate thermal expansion, etc.) and in a variety of forms for numerous applications (IR domes, laser windows to optic fibers, smart panels, sealants for the SOFC, biomaterials, etc.) [1-5].

Knowledge of the glass structure is essential in comprehending their physicochemical properties and hence in optimizing compositions and synthesis conditions [2]. Studying of the composition effect and glass structure leads to insights of the glass properties as glass transition, T_g, thermal stability, and electrical conductivity. If the thermal properties (Tg, glass stability, etc.) enhances when the content of the glass forming oxides (SiO_2, B_2O_3) increases, the effect of the glass modifiers is opposite [6]. Distinct effect of the network modifiers on glass network structure by creating non-bridging oxygens, NBOs, depends on their field strength, ionic radius, polarizability and coordination number.

Conversely, electrical conductivity of solid silicate glasses has an intricate dependence on glass composition, devitrification, and temperature [6,7]. Small change in the glass composition can trigger notable differences in the electrical conductivity values [8]. However, the experimental data on the electrical conductivity of the glasses and slags are rather scarce [9,10] and mostly reported for binary systems [7]. Although, extensive theoretical models have been developed the mixed alkali effect in ion conducting glasses is still controversial [4]. Therefore, it is necessary to investigate the influence of the metal oxide on electrical conductivity of the multi-component silicate glasses for electrical purposes (solid-state batteries, fuel cells, chemical sensors and smart windows [4]).

The aim of this work is to obtain by quench method and study the crystallization behavior and microstructure of several compositions in the SiO_2-Al_2O_3-MeO-M_2O system (were M stand for Na, K while Me represent Mg, Ca, Ba) by means of DSC, X-ray diffraction, SEM-EDS and Raman spectroscopy. Further, the electrical conductivity measurements are discussed in terms of the structural findings.

2. Experimental

2.1 Materials and glass elaboration

The reagent grade chemicals, Na_2CO_3 (Reactivul Bucharest), K_2CO_3, $CaCO_3$ (Reactivul Bucharest), $BaCO_3$, $MgCO_3$, Al_2O_3 and SiO_2, (Merck) were used as starting materials to prepare by melt quenching the five silicate glasses in the M_2O-MeO-Al_2O_3-SiO_2 system (M=Na, K and Me=Ca, Mg and Ba, respectively) listed in Table 1. Appropriate amounts of the reactant mixtures were weight, homogenized and melted at 1450-1500 °C for 2 hours and

10 hours for the 15K composition, respectively. The melts were finally quenched in air. These glasses were used for electrical conductivity in solid state and their powder was used for DSC measurements.

Table 1. Glass compositions

Sample	Component (wt. %)						
	SiO_2	Al_2O_3	MgO	CaO	BaO	Na_2O	K_2O
20Mg	60	5	20	-	-	15	-
20Ca	60	5	-	20	-	15	-
20Ba	60	5	-	-	20	15	-
15K	60	5	-	20	-	-	15
12Ba	70	4	-	-	12	7	7

2.2. Thermal analysis

The thermal measurements were carried out on a SETARAM LabSys Evo-1600 system operating in standard mode within 25–1500 ^oC under argon atmosphere. Calisto V1.051 software was used for data acquisition and primary signal processing. Samples of 26–28 mg were placed in platinum and their thermograms were collected with a 10 ^oC/min rate on heating. Since no routine fitting procedure is known for DSC peaks except for the modulated DSC, spectroscopic and chromatographic elements were used to analyzing overlapped, asymmetric peaks by means of the PeakFit software [11] with a Haarhoff-Van der Linde band profile.

2.3 X-ray diffraction

X-ray diffractograms were collected by means of a Rigaku diffractoctomer type Ultima IV in parallel-beam geometry. The X-ray from a Cu tube operating at 40 kV and 30 mA. Counts were collected from 5^o to 70^o with a step size of 0.02 and a speed of 5^o/min.

2.4 Raman spectroscopy

Unpolarized solid state Raman spectra were recorded by means of a LabRam HR spectrometer (Jobin-Yvon–Horiba) over 50-1400 cm^{-1} range. The 514 nm line of an Ar^+ laser was used as exciting radiation through a 50× objective of an Olympus microscope in a backscattering geometry and at a confocal hole of 200 μm. The diameter of the laser spot on the sample surface amounted to 2–3 mm providing a spectral resolution better than 2 cm^{-1}. The resulted spectra were background corrected [12] and curve fitted by Gaussian profile (except for the boson peak with log-norm profile) using an Igor software [13]. The fitting residuals were kept bellow 2 %.

2.5 SEM

The crystallization characteristics and internal microstructures of the resultant materials were examined by scanning electron microscopy (SEM), where representative electron micrographs were obtained using a Jeol JSM 6100 Electron Probe Microanalyzer coupled with Energy Dispersive Spectrometer (EDS) KEVEX Quantum operating at 20 kV. The raw and devitrified samples for the Scanning Electron Microscopy (SEM) and Electron Dispersive Spectrometry (EDS) measurements were obtained by heat treatment for 24 h at 800 ^oC.

2.6. Electrical conductivity

The electrical conductivity of the glasses under discussion was measured by using an experimental set up developed at the CEMHTI Orleans [14]. The experimental set-up was composed of an electrical-heated tube furnace (diameter of 10 cm and length of 15cm) reaching up 1770 K temperature. It allows measuring of the temperature within [373-(T_g+50) K] interval (T_g stands for the glass transition temperature) in a frequency domain of 100Hz-10 MHz. The device is based on a pseudo 4 point-method, provided with an impedance spectrometer HP 4194A and a Lab View program for data acquisition. The sample impedance is wireless recorded. A Pt/Pt-Rh10% thermocouple in the proximity of the sample (<1mm) is used for recording temperature of the sample. For a certain temperature T, the complex impedance of the sample is measured as a function of frequency (ω) by following: $Z^*(T,\omega) = R(T,\omega) + jX(T,\omega)$, where the two terms of the equation represent the resistance and the reactance of the sample respectively. The samples consisting in glass disks (diameter of 10 mm and thickness of about 1 mm) have the two faces optically polished and platinum coated. Knowing the geometric factor of the sample (l/s=thickness/surface of an electrode), the complex conductivity is: $\sigma^* = l \cdot Z^* / s$. The LabVIEW software allows simultaneous acquisition of frequency, temperature and complex impedance Z*(T, ω) of the sample.

3. Results

3.1 Crystallization behavior

The multicomponent crystallization exotherms of the DSC scans for as-quenched glasses are shown in Fig. 1. Results of the DSC exotherm decomposition and the X-ray phase identification of the thermal treated samples for 24 h at the corresponding exotherm of crystallization are summarized in Table 2.

The major phases corresponding to the two-component decomposition of the DSC exotherms of crystallization for the 20Mg glass are: albite ($NaAlSi_3O_8$) and (SiO_2) at 710 ^oC and albite at 766 ^oC. Above 1000 ^oC (inset of the Fig. 1), the 20Mg glass shows an additional weaker exotherm (almost three times weaker than the one peaking up at 766 ^oC) also fitted with two components located at 1092 and 1135 ^oC. The high temperature exotherms are tentatively assignable to the magnesium metasilicate, $MgSiO_3$ [15]. Although, extensive investigation of the $MgSiO_3$ (enstatite) was trigged by its abundance in the Earth's lower crust and upper mantle [15], however precise stoichiometric composition of enstatite does not result in a stable glass.

The DSC exotherms of crystallization for the two containing barium glasses, 20Ba and 12Ba respectively, were decomposed into three components (Fig 1 and Table 2) according to the DSC signal derivative. If the first two components, assignable to the $Ba_2Si_4O_{10}$ and the orthosilicate (Na_4SiO_4), are similar for the two glasses (Fig. 2), the third one is 14 ^oC shifted towards higher temperature in the case of 12Ba. The latter exotherm of the 20Ba glass was assigned to the orthorhombic sanbortite ($BaSi_2O_5$) resulted by transition of the monoclinic $Ba_2Si_4O_{10}$. Traces of silimanite, $BaSi_2O_5$, are depictable in the X-ray diffractogram of 20Ba devitrified for 24 h at the temperature of the third exotherm. In comparison to the 20Ba glass, the 12Ba glass devitrified at 792 ^oC (incomplete devitrified glass during the 24 h span, Fig. 2b) shows two major crystalline phases Al_2SiO_5 and a monoclinic $Ba_3Si_5O_{13}$.

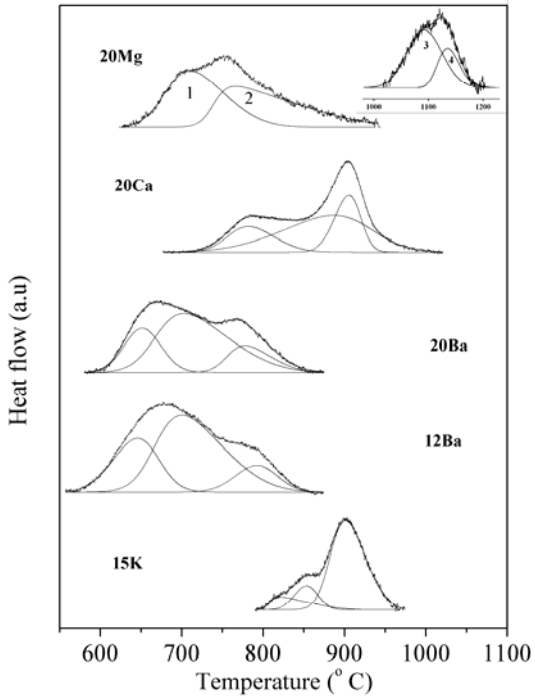

Fig. 1 DSC exotherms of crystallization for the 20(Mg/Ca/Ba), 12Ba and 15K glasses (inset represents DSC exotherms of the 20Mg within 1000-1200 ^oC)

The three-component model was used to decompose the crystallization exotherms for 20Ca and 15K glasses with the same composition but with different alkaline oxide, Na_2O for 20Ca and K_2O in case of 15K. According to the X-ray findings, combeite ($Na_2Ca_2Si_3O_9$), wollastonite ($CaSiO_3$) with combeite and nepheline ($NaAlSiO_4$) with combeite were formed as major crystalline phases in the devitrified 20Ca glass at 782, 887 and 905 ^oC, corresponding to the three exotherms in Fig. 1. Traces of nepheline were also depicted from X-ray data of the glass crystallized at 887 ^oC. Combeite-based glasses and glass-ceramics received much attention lately due to its potential use as bioactive material [5,16]. However formation of the nepheline phase is incriminated for severe deterioration of the chemical durability in sodium- and aluminum-rich high-level nuclear waste glasses [17,18]. As for the 15K glass, where Na_2O was replaced by K_2O (Table 1), leucite ($KAlSi_2O_6$) is identified in the devitrified sample at 853 ^oC while at higher temperature (901 ^oC) sanidine ($KAlSi_3AlO_8$) came out. Analog to preparation of the potassium lime silicate glasses at about 1600 ^oC in open systems where severe volatilization of K_2O takes place [18], the $K_2Ca_2Si_2O_7$ represents the major phase formed at 821 ^oC of the first crystallization exotherm for the 15K glass. These glass and glass-ceramics were reported as ceramic restoration materials [16-18].

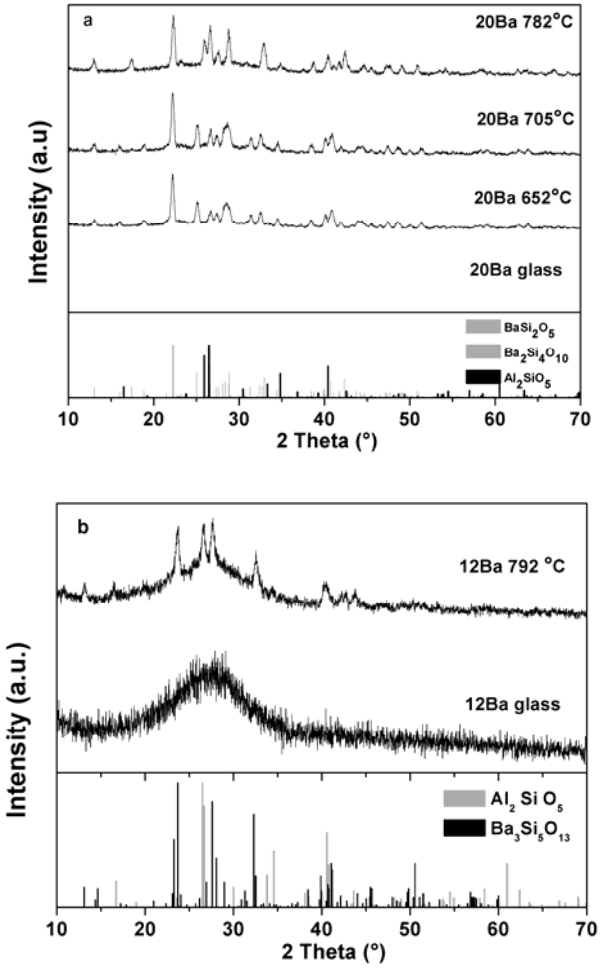

Fig. 2 X-ray diffractograms of the barium-containing glasses : (a) 20Ba and (b) 12Ba

Table 2. Characteristic temperatures of the decomposed DSC exotherms of crystallization within 600-1000 °C, the difference T_{on} - T_g for the investigated glasses and major phases identified by X-ray measurements in the devitrified samples

Sample	T_g (ºC)	exotherm	T_{on} (ºC)	T_p (ºC)	T_{on}-T_g (ºC)	Major phases	JCPDS card no.
20Mg	505	1	652	710	147	quartz (SiO_2)+albite ($NaAlSi_3O_8$)	00-046-1045+ 01-071-3816
		2	722	766	217	$NaAlSi_3O_8$+ SiO_2	01-071-3816+ 00-046-1045
20Ca	586	1	732	782	146	combeite($Na_4Ca_4Si_6O_{18}$)	01-075-1687
		2	760	887	174	combeite+wollastonite ($CaSiO_3$)	01-075-1396
		3	870	906	284	combeite+nepheline ($NaAlSiO_4$)	00-035-0424
20Ba	502	1	607	651	105	$Ba_2Si_4O_{10}$+ Na_4SiO_4	01-071-0797 + 00-032-1154
		2	638	703	136	$Ba_2Si_4O_{10}$	01-071-0797
		3	737	778	235	sanbornite ($BaSi_2O_5$)	01-072-0171
12Ba	475	1	586	646	111	$Ba_2Si_4O_{10}$+ Na_4SiO_4	01-071-0797+ 00-032-1154
		2	638	701	163	$Ba_2Si_4O_{10}$	01-071-0797
		3	739	792	264	sillimanite (Al_2SiO_5) + $Ba_3Si_5O_{13}$	01-074-0274+ 00-026-0179
15K	710	1	798	821	88	$K_2Ca_2Si_2O_7$	[18]
		2	823	853	113	$CaSiO_3$+ leucite ($KAlSi_2O_6$)	01-076-0925+ 00-015-0047
		3	865	901	155	sanidine ($KAlSi_3AlO_8$) +$CaSiO_3$	01-071-1544+ 01-076-0925

Ton and Tp stand for the onset and peak temperatures of crystallization

3.2 Raman spectra and assignments

Raman spectra for all the five glasses, the 20(Mg/Ca/Ba), 12Ba and 15K glasses, are illustrated in Fig. 3 while the Raman deconvolution results are listed in Table 3.

Raman spectra of the alkali and alkaline-earth silicate glasses are divided into three regions namely: (i) region below 400 cm^{-1} is due to the lattice modes (boson peak) and the network modifying cations (Na^+, K^+, Mg^{2+}, Ca^{2+} and Ba^{2+} in this work) and is in relation to long-range order, (ii) region between 400 and 800 cm^{-1} corresponding to Si–O–Si bending vibrations within inter–tetrahedral linkages and (iii) above 800 cm^{-1} due to the Si–NBO stretching modes of mainly silicate units, Q^n (where n stands for 0, 1,2, 3 and 4) [12,20,21]. The Q^n units were included into five classes in accordance to their non bridging oxygen per network forming tetrahedral ratio (NBO/T) equal to: 4 (Q^0: SiO_4), 3 (Q^1: $Si_2O_7^{6-}$), 2 (Q^2: $Si_6O_{18}^{12-}$ and $Si_2O_6^{4-}$), 1 (Q^3: $Si_4O_{11}^{6-}$ and $Si_2O_5^{2-}$) and 0 (Q^4: SiO_2).

3.2.1 Region below 400 cm^{-1}

At low frequencies, the lattice modes are sometimes affected by the presence of larger cations (Na^+, K^+, Ca^{2+} and Ba^{2+} of 1.2, 1.38, 1.02 and 1.35 Å ionic radii) and their translational modes metal-oxygen. Although the origin of so-called boson peak (BP) is still a matter of debate [19], presence of the BP is a signature of the glassy nature of the investigated material. The lowest position of the BP is recorded for 20Mg and 15K glasses. The other three weak bands in this region are related to the glass modifying cation modes (Fig. 2a). The band at about 320 cm^{-1} for 20Mg and 20Ba glasses shifted toward higher wavenumbers, 359 cm^{-1}, when Mg^{2+} and Ba^{2+} respectively were replaced by Ca^{2+} in the 20Ca and 15K glasses (Table 3). This means that stronger coupled vibration of Ca–O and SiO_4 network is encountered.

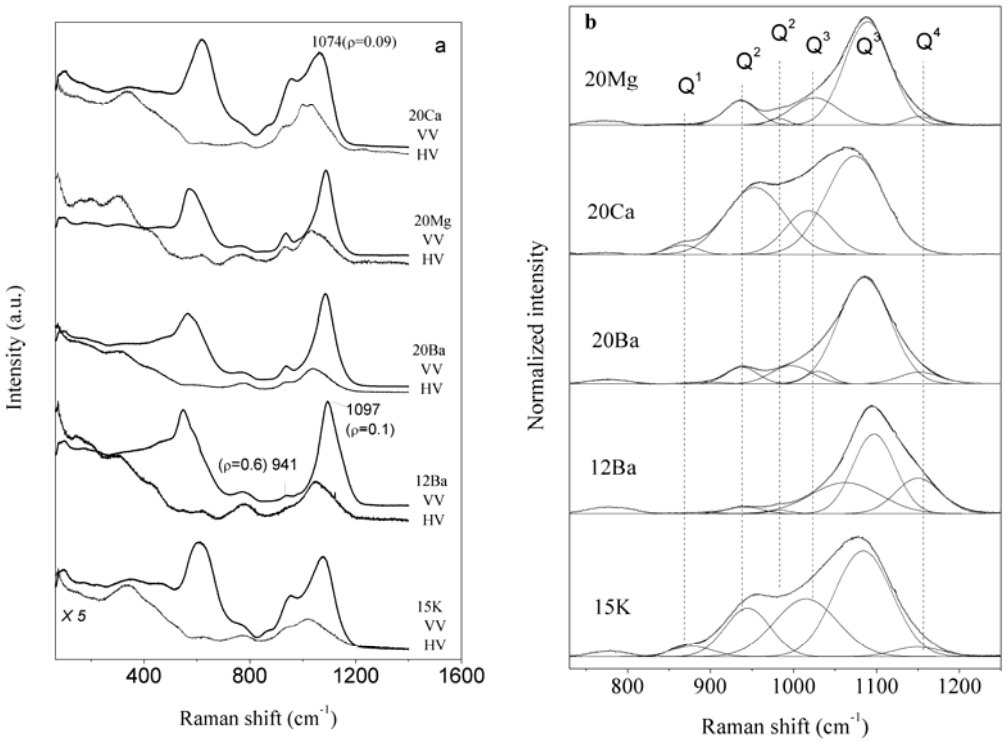

Fig. 3 Raman spectra of the 20(Mg/Ca/Ba), 12Ba and 15K glasses: (a) vertical (VV) and horizontal (HV) polarized (ρ stands for depolarization ratio, I_{HV}/I_{VV}) and (b) deconvoluted within 730-1250 cm^{-1}

The presence of the 162 and 204 cm^{-1} bands in the devitrified 20Mg glass (Fig. 4) at the temperature of the second exotherm of crystallization are assignable to the ν(Na-O) in albite ($NaAlSi_3O_8$) [22]. Bands at 82 and 105 cm^{-1}, also depictable in Fig. 4 of the VV spectrum for devitrified 20Mg, were used for identification of the low temperature polymorphs of crystalline enstatite: ortho- and clino-enstatite [23].

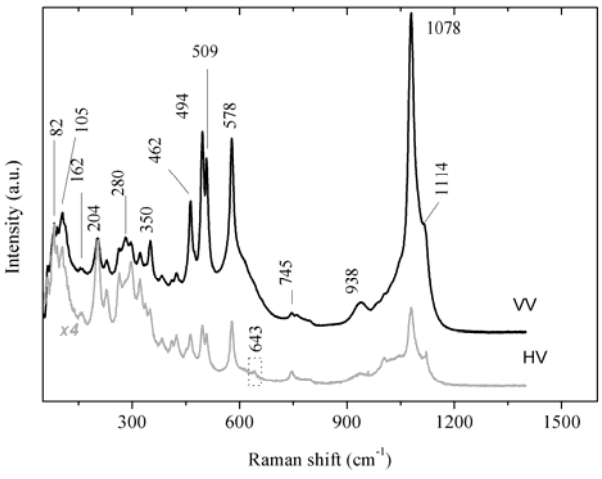

Fig. 4 VV and HV Raman spectra of the devitrified 20Mg glass at 766 °C for 24 h.

3.2.2 Region within 400-800 cm^{-1}

Bands located in the mid-frequency region are related to the vibrations of the anionic units. Both glasses with K_2O in their compositions, 12Ba and 15K (see Table 1), have a band at about 588 and 584 cm^{-1}, respectively (Fig. 2) which was also reported for amorphous sanidine ($KAlSi_3AlO_8$) [22] already identified in the devitrified 15K composition (Table 2). Analog to the crystalline albite ($NaAlSi_3O_8$) with a strong doublet at 508 and 479 cm^{-1} [22], bands at 462, 494 cm^{-1} in the Raman spectra of the devitrified 20Mg in Fig. 4 (almost 15 cm^{-1} shifted towards lower wavenumbers) can be assigned to the same compound. Lower wavenumber shifted doublet 636 and 643 cm^{-1} in Fig. 4 can be tentatively assigned to the low temperature polymorphs of enstatite, typically located within 663-685 cm^{-1} [23]. The band located around 770 cm^{-1} can be assigned simultaneously to Si-O-Si network and AlO_4 tetrahedra. Since Al_2O_3 content of all the glasses under discussion does not exceed 5 wt. % as depictable in Table 1, it is assumed that all aluminum ions are located in tetrahedral sites.

3.2.3 Region within 800-1200 cm^{-1}

Except for the band located within 1020-1040 cm^{-1} with double assignment (see Table 3), the high frequency region is related to the symmetric stretching modes of the Q^n species and it is used for quantification of the Q^n abundance according to integrated Raman bands suggested by Mysen [21]. In our case, four to six components were

used for fitting these wide and intense bands. Comparing the calcium oxide containing glasses, 20Ca and 15K, the 20Ca glass does not contain Q^4 units or their small quantity is obscured by the strong 1074 cm^{-1} band. The 20Mg and 20Ba glasses encountered for 4.45 and 6.34 % Q^4 population, respectively. The biggest Q^4 population was derived for 12Ba glass with the biggest SiO_2 content.

Table 3 Decomposition results (peak position/FWHM and Q^n population) and band assignments [12, 19-21] of the Raman spectra for the 20(Mg/Ca Ba), 15K and 12 Ba glasses

20Mg (cm^{-1})	20Ca (cm^{-1})	20Ba (cm^{-1})	12Ba (cm^{-1})	15K (cm^{-1})	Assignment
<400 cm^{-1}					Latice modes and cation related vibrations
96/34	99/57	97/58	98/50	96/49	Lattice modes (boson peak)
182/33	165/74	172/83	175/81	166/73	vibration of network modifying cations (Na^+/K^+)
221/36	225/30	227/35	228/35	225/26	vibration of network modifying cations ($Mg^{2+}/Ca^{2+}/Ba^{2+}$)
320/67	359/103	329/88	312/76	359/116	Coupled vibration of Me–O and SiO_4 network
400-800 cm^{-1}					Vibrations of the anionic units
459/39	459/40	450/53	456/55	463/61	400-650 cm^{-1} bending vibrations of the bridging oxygen (BO) bonds of SiO_4
565/48		557/61	547/42		
			588/53	584/59	
605/84	621/97	602/84	637/53	634/77	
771/50	771/32	777/60	779/64	778/46	Si–O–Si network and AlO_4 units with three BOs and one NBO
800-1200 cm^{-1}					Symmetric vibrations of the Q^n species (n=1, 2,3 and 4)
859/55 (0.48 %)	866/43 (2.38 %)	891/58 (0.95 %)	887/51 (0.59 %)	878/58 (3.33 %)	890-950 cm^{-1}, $\upsilon_{Si\text{-}O}$ in paired tetrahedra ($Si_2O_7^{6-}$): Q^1
936/47 (11.06 %)	954/83 (32.86 %)	938/45 (6.96 %)	941/49 (3.16 %)	945/64 (17.10 %)	930-1000 cm^{-1}, $\upsilon_{Si\text{-}NBO^*}$ in chain ($Si_2O_6^{4-}$):Q^2
981/28 (1.86 %		997/57 (9.46 %)	983/34 (1.11 %)		
1025/66 (17.57 %)	1018/65 (16.81 %)	1030/36 (4.26 %)	1063/99 (28.91 %)	1015/89 (28.40%)	ν (Si–NBO) in Q^3 and/or asymmetric stretching of BOs related to the Q^1-Q^3 units
1089/65 (65.58 %)	1074/83 (47.95 %)	1086/73 (72.03 %)	1097/60 (44.95 %)	1084/81 (47.51%)	1020-1100 cm^{-1}, Q^3 ($Si_2O_5^{2-}$ sheet)
1152/42 (3.45 %)		1152/58 (6.34 %)	1150/63 (21.28 %)	1150/67 (3.66 %)	1150-1200 cm^{-1}, Q^4 (SiO_2 framework)

Literature NMR estimation of the Q^n populations in enstatite glass (1.4 for Q^0, 19.1 for Q^1, 53 for Q^2, 25.2 for Q^3 and 1.4 % for Q^4) and forsterite glass (62.9 for Q^0 and 37.1 % for Q^1) [24] are rather different than the ones met in the 20Mg glass (Table 3). This is probably due to small content of these magnesium silicate compositions in the 20Mg glass. In the devitrified 20Mg specimen at 766 °C, forsterite did not crystallized since its two intense A_g bands at 825 and 856 cm^{-1} of the independent SiO_4^{4-} anions [19] are not noticeable in the polarized spectra in Fig. 4. Otherwise, stretching Si–O vibrations above 1000 cm^{-1} of the crystalline enstatite, sensitive to the crystal orientation [23], could be included in strong bands the 1078 and 1114 cm^{-1} along with albite and quartz (Fig. 4).

The Q^3 population in the borosilicate glasses was found to be a controlling factor of corrosion resistance and volatilization from the melts [25]. All the depolarization ratios (ρ) of the Q^n units are bellow 0.75 value which is the maximum value for the fully symmetric vibration modes. For instance, the 12Ba glass has ρ of 0.6 for Q^2 and comparable values for Q^3 and Q^4 units of 0.1 and 0.2 (Fig. 3).

3.3 SEM

The SEM micrographs of the devitrified 20Mg, 20Ca and 12Ba glasses annealed at 800° C for 24 h are illustrated in Fig. 5.

The gray crystals in micrograph 4a are unevenly distributed at the surface of the 20Mg specimen. The firing temperature is the intermediate crystallization temperature of albite ($NaAlSi_3O_8$) and enstatite ($MgSiO_3$) exotherm of crystallization. In accordance to the X-ray diffraction (XRD) findings for 20Mg devitrified at 800 °C (not shown in this work) the crystalline phase was assigned to the enstatite. During annealing at temperatures ≥ 800 °C for 24h the forsterite (Mg_2SiO_4) converts to enstatite according to the following reaction: $Mg_2SiO_4+SiO_2 \rightarrow 2MgSiO_3$.

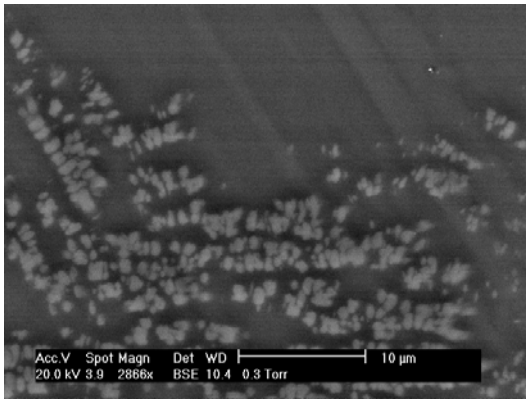

a

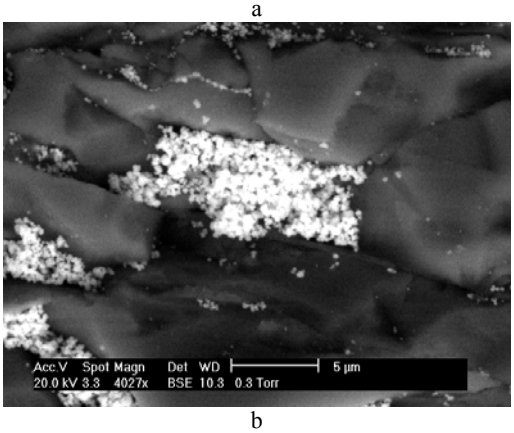

b

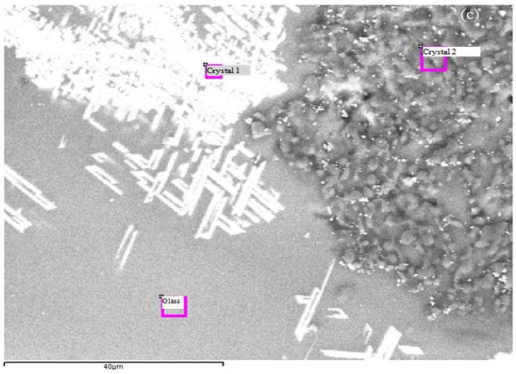

c

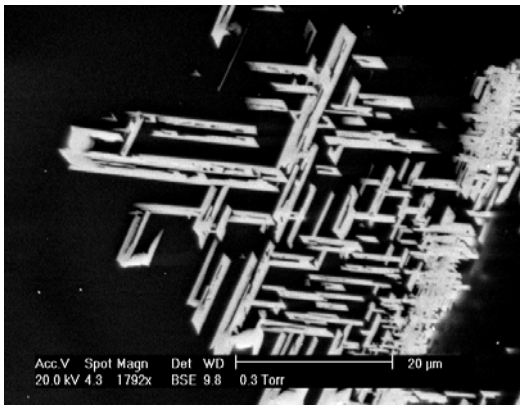

d

Fig. 5 SEM micrographs of the: (a) 20Mg (10 µm), (b) 20Ca (5 µm), (c) 12Ba (40 µm) and (d) 12Ba (secondary electron image of crystal 1, 20 µm) specimens crystallized at 800 °C for 24 h.

At 800° C, between first two crystallization exotherms of the 20Ca glass (Fig. 1), two major crystalline phases were formed by devitrification, namely combeite ($Na_4Ca_4Si_6O_{18}$) and wollastonite ($CaSiO_3$). The EDS analysis of the matrix in Fig. 5b gave a Si:Na ratio about 4 while the Si:Ca is almost 2:1, exceeding the values for crystalline combeite (Si:Na=1.5) and wollastonite (Si:Ca=1). Hence, the surrounding matrix of the tiny crystals of combeite and wollastonite (confirmed by X-ray diffraction, XRD) is mostly silicate one. Due to the submicron size and clustering of the crystals in the micrograph 5b, higher magnification could help to detect the shape of the resulted crystals [26].

The darker and smaller crystals in Fig. 5c of the 800 °C annealed 12Ba belong to the barium derived material (probably $Ba_3Si_5O_{13}$ according to the XRD data). The surrounding matrix of the two type of crystals is a silicate one. The giant prismatic shaped crystals in Fig. 5d for the same 12Ba crystallized at the third exotherm in Fig. 1, correspond to sillimanite (Al_2SiO_5) as depicted by the XRD findings. Besides, the Al:Si ratio close to 2:1 from EDS analysis of these crystals confirms the presence of sillimanite as giant crystals in the devitrified 12Ba at 800 °C.

3.4 Electrical conductivity

The electrical conductivity, σ, in solid state was measured as a function of frequency, ω, and temperature for all glasses under discussion. The temperature limits were imposed by the experiment and sample (the lower one by the high resistance of the sample and the upper one by the Tg). The obtained electrical conductivity curves versus frequency are typical for ionic conduction. They obey the UDR law (Universal Dielectric Reply) [10]: $\sigma(\omega) = \sigma_{dc} + A\omega^s$ where first term is the static conductivity, ω is the frequency, A and s are phenomenological parameters temperature dependent.

The frequency dependence of the electrical conductivity obtained with the solid state setup is shown in Figs. 6 and 7 for 20Mg and 20Ca glasses at some selected temperatures. As noticeable, increasing frequency and temperature is accompanied by an increase of the electrical conductivity. However there is a limit, called ω_1, to a certain temperature and modifying divalent oxide, where the electrical conductivity curves become parallel and hence frequency independent.

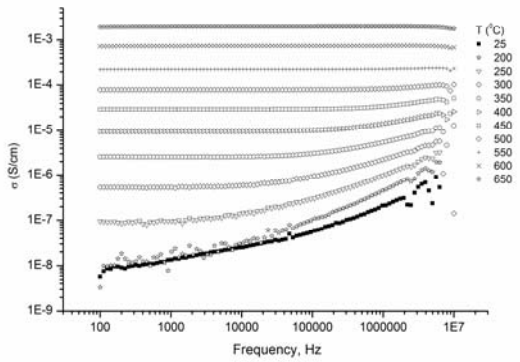

Fig. 6 Frequency dependant electrical conductivity of the 20Ca glass.

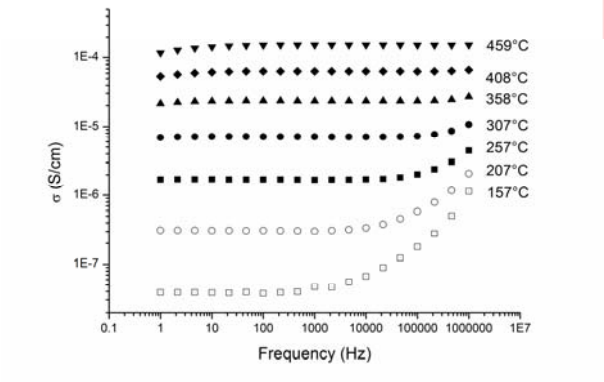

Fig. 7 Frequency dependant electrical conductivity of the 20Mg glass.

All studied glasses have a similar behavior, i.e. the static conductivity (σ_{dc}) obeys the Arrhenius law characteristic for the thermal activated ionic transport, as can be seen in Fig. 8. The electrical conductivity decreases in the following sequence: 20Mg> 20Ba> 20Ca> 12Ba> 15K. The calculated activation energies for all the five glasses increased in the reversed order except for the 20Mg and 20Ba glasses.

The transport mechanism for the electrical conductivity in these glasses below their glass transition temperatures is ionic and is realized by the alkali ions and/ or Mg^{2+} ions located in tetrahedral environments. These ions can move in the less compact regions of the glass.

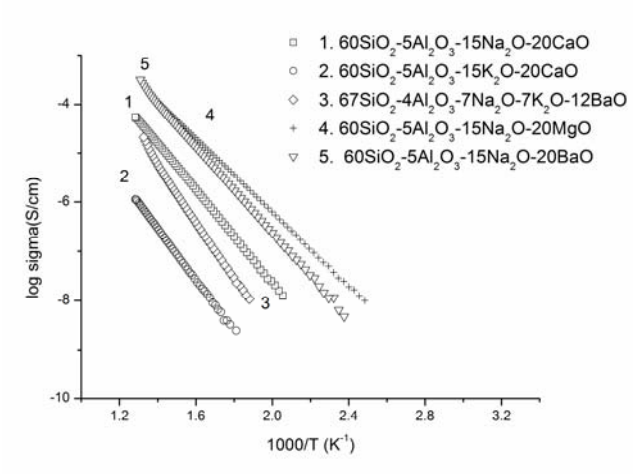

Fig. 8 Temperature dependence of the electrical conductivity in silicate glasses studied

Table 4. Arrhenius fit of the electrical conductivity data for the 20(Mg/Ca/Ba), 12Ba and 15K glasses

Glass	σ (S/cm)	E_a (KJ/mol)	R^2	ΔT (K)
15K	Log σ=1.53-5.76364(10^3/T)	110.21	0.9924	555-800
12Ba	Log σ=2.50176-5.55924(10^3/T)	106.28	0.9979	532-770
20Ca	Log σ=2.04442-4.83435(10^3/T)	92.43	0.9973	488-770
20Mg	Log σ=1.37567-3.80419(10^3/T)	72.72	0.9939	417-770
20Ba	Log σ=2.12811-4.33784(10^3/T)	69.14	0.9988	417-745

4. Discussion

4.1 Composition effect on network connectivity and thermal stability

Network connectivity of the silicate glasses is better described by the Q^n species (anionic species) while the cationic environment, i.e. coordination number and cation-network interactions, is an important parameter to establish the mechanism of the ion transport in silicate systems. The Q^n species are associated with the *n* BOs in Si-O-Si bridges and (4-*n*) NBOs in $(\equiv Si-O^{-}\cdot\cdot)$ species compensated by alkali ions (in this case: Na^+ and K^+) and/or alkaline-earth ions (here, Mg^{2+}, Ca^{2+} and Ba^{2+}). In a silicate glass, the Q^3 and Q^4 species are responsible for the higher network connectivity. These anionic species was derived by fitting of the high frequency Raman bands (Figs 3b) for the 20(Mg/ Ca/ Ba), 12Ba and 15K glasses. Sum of the Q^3 and Q^4 populations, corresponding the last two bands in Table 3, for the glasses with the same MeO content (20 wt. %) and the same Na_2O/SiO_2 ratio (Table 5) decreases in the following sequences: 20Ba> 20Mg> 20Ca. However, the fraction of the NBOs calculated from the molar composition enhances in the 20Mg> 20Ba> 20Ca succession as the sum of the mobile species (Q^1 + Q^2). A plausible explanation of this behavior consists in the different coordination environments of the small Mg^{2+} cations [19] and mixed alkali effect. Recent ^{25}Mg MAS NMR data [28] pointed out a preferential octahedral coordination of Mg^{2+} and that MgO_6 octahedra contribute to the network formation by weak covalent bondings [19] and hence validity of the equation for f_{NBO} calculation is somehow limited for the 20Mg glass.

Overall the Q^3 and Q^4 abundance and hence degree of network polymerization decreases as following: 20Ba> 20Mg> 12Ba > 15K> 20Ca. The more polymerized network in barium- and magnesium-containing glasses, the higher thermal stability encountered in these glasses. In fact, all the glasses presented here, except for the 15K (first exotherm of crystallization), have the difference between the onset of the crystallization temperature, T_{on}, and the glass transition temperature, T_g, higher than 100 °C (Table 2) and hence a good thermal stability. Although the MgO_6 are weakly bonded to the silicate network, they caused the 20Mg glass to have a bigger difference T_{on}-T_g. The peculiar behavior of the 20Mg glass can be attributed to the amphoteric character of the Mg^{2+}, meaning at least

two coordination numbers (4 and 6 respectively) were adopted by the Mg^{2+} ions with an ionic radius (0.72 Å) smaller than critical value of 0.872 Å [29]. These cations with high charge and small ionic radius also can adopt a 4-fold coordination being able to polarize their neighboring oxygen towards themselves producing bonds with a stronger covalent character.

Due to the fact that populations of the Q^1 species, mobile ones, are relatively low in the 20(Mg/ Ca/ Ba), 12Ba and 15K glasses (see Table 3), volume nucleation is less favored in these glasses. Higher Q^1 abundance was recorded the two 20Ca and 12K glasses, the glasses containing CaO as alkaline-earth glass modifier and with the biggest f_{NBO} (Table 5).

Table 5. Molar ratio glass modifying oxide/glass forming oxide and fraction of NBOs

Glass	f_{NBO}	MeO/SiO_2	M_2O/SiO_2	
			M=Na	M=K
20Mg	0.24	0.5	0.241	-
20Ca	0.4	0.3571	0.241	-
20Ba	0.26	0.1306	0.241	-
15K	0.35	0.3571	-	0.159
12Ba	0.17	0.067	0.096	0.063

*$f_{NBO}=2\cdot(cM_2O+cMeO-cAl_2O_3)/(2\cdot cSiO_2+3\cdot cAl_2O_3+cMeO+cM_2O)$ [27], where c is the molar composition

4.2 Network modifying cations effect on the electrical conductivity

The cationic environment, i.e. coordination number and cation-network interactions is an important parameter to establish the mechanism of the ion transport in silicate systems. Moreover, electrical conductivity of both solid silicate materials is highly sensitive to temperature, chemical composition and devitrification mechanism [28]. Typically, alkali and alkaline-earth modifiers oxides play either the role of glass modifiers and cause silicate network depolymerization being bonded to NBOs, or charge compensators, near the AlO_4 tetrahedra, bonded with BOs. In fact, the combination way of the M^+ and Me^{2+} cations with the NBOs in Q^n species, but Q^4, changes as the coordination number of these cations, CN, change [30]. Although, larger Me^{2+}cations (in this case Ba^{2+}) prefers association with more open Q^3 species in sheets and small cations, Mg^{2+}, favor to associate with Q^2 species in chains, no reasoning was provided for this behavior [30].

Even if the electrical conductivity of the 20(Mg/ Ca/ Ba) glasses with the same Na_2O/SiO_2 ratio decreases in the same sequence as the f_{NBO} (Table 5) and the mobile species (Q^1+Q^2 in Table 3), i.e. 20Mg> 20Ba> 20Ca, their E_a values (Table 4) increase in a reversed order than summation of Q^3 and Q^4 speciation: 20Ba< 20Mg< 20Ca. Therefore, the transport mechanism in these materials is different. While Na^+ ions are charge carriers in solid glasses, the bivalent ions, except for Mg^{2+} [9], are involved in a cooperative motion through the network. According to the Hudon model [31], the cation charge appears to play no role in selection of cations able to adopt 4-fold coordination as Mg ions. The covalent bonding is expected to shield the modifier cations, reducing the coulombian repulsions with other cations. Moreover, the amphoter Mg^{2+} ion is also possible to participate in electric conduction along with Na^+ ions (Fig. 8), their movement being facilitated by the more depolymerized networks with bigger mobile populations, Q^1 and Q^2. Reversed order in the E_a values for 20Mg and 20Ba glasses in comparison to the electrical conductivity values is based on the different association preferences of the Mg^{2+} and Ba^{2+} ions for NBOs in the Q^2 and Q^3 species, respectively [30]. These species, organized in chains and sheets, respectively give different compactness of the silicate network [32].

Given the fact strongly dependence of the electrical conductivity on the size of the of the alkali ions, considered the only charge carriers in alkali silicate glasses, presence of the large K^+ ions induces a decrease of the (σ_{dc}) for the 12Ba and 12K glasses. Hence, the ionic radius of the charge carriers is an important parameter in electric conduction in solid glasses. Bigger activation energies observed in the 12Ba and 15K glasses can be also explained by the larger ionic radius of K^+.

5. Conclusions

Structural and thermophysical characterization of five 20(Mg/Ca/Ba), 15K and 12Ba glasses were achieved. Decomposition of the overlapped and asymmetric DSC exotherms of crystallization was performed with two components for 20Mg and three components for the rest of the glasses. Good thermal stability was recorded for the 20(Mg/Ca/Ba) and 12Ba glasses, except for the 15 K glass. Raman investigations of the 20Mg glass devitrified at 800 ^oC allowed identification of the low temperature enstatite polymorphs. Electrical conductivity of the 20(Mg/ Ca/ Ba) glasses was explained in terms of the size and coordination of the Me^{2+} ions as well as compactness of the silicate network. Peculiar behavior of the 20Mg glass concerning fraction of the non-bridging oxygen, f_{NBO}, and network connectivity (summation of the Q^3 and Q^4 species) is caused by partial formation of the MgO_6 octahedra weakly bonded to the silicate network. Presence of the large K^+ ions in the 20Ca and 15K glasses caused sudden decrease of the electrical conductivity and increased glass transition temperature. However, due to the different concentrations and type of the glass modifying components of the quaternary glass compositions under discussion, it is difficult to have a univocal explanation solely based on Q^n species and/ or alkaline-earth cation size.

Acknowledgments

Partially support of the EU (ERDF) and Romanian Government that allowed for acquisition of the research infrastructure under POS-CCE O 2.2.1 project INFRANANOCHEM - Nr. 19/01.03.2009, is gratefully acknowledged. Authors are thankful to Dr. E.Veron from

CEMHTI, Orleans for the SEM-EDS measurements within CNRS-Romanian Academy cooperation.

References

[1] R.K. Brow, M.L. Schmitt, J. Eur. Ceram. Soc. **29**, 1193 (2009).
[2] D.R.Neuville, L.Cormier, D. Masiot, Chem. Geol. **229**,173 (2006).
[3] L.Cormier, G. Calas, B.Beuneu, J. Non-Cryst. Solids **357,** 926 (2011) .
[4] A. Dutta, T.P. Sinha, P. Jena, S. Adak, J. Non-Cryst.Solids **354**, 3952 (2008).
[5**]** R. Du, J. Chang, J. Mater. Sci.: Mater. Med. **15**, 1285 (2004).
[6] Y. Zhao, C. Ning, J. Chang, J. Sol-Gel Sci. Technol. **52**, 69 (2009).
[7] H.Scholze, Glass Nature, Structure, and Proprieties, Springer Verlag, New York, 1991.
[8] G-H. Zhang, B-J. Yan, K-C. Chou, F-S. Li, Metall. Mater. Trans. B **42B**, 261 (2011).
[9] B.T. Poe, C. Romano, V. Varchi, V. Misiti, P. Scarlato, Chem. Geol. **256**, 193 (2008).
[10] M. Ma1ki, M. Constantinescu, P. Echegut, C.Bessada, I. Nuta, R. Piper, M. Olteanu, Glass Technology **46**, 146 (2005)
[11] V.T**.** Popa, E. Segal, J. Therm. Anal. Calorim. **69**, 149 (2002).
[12] L. Robinet, A. Bouquillon, J. Hartwig, J. Raman Spectrosc. **39**, 618 (2008).
[13] E. Buixaderas, E.M.Anghel, S. Petrescu, P.Osiceanu, J. Solid State Chem. **183**, 2227 (2010).
[14] M. Malki, P. Echegut, J. Non-Cryst. Solids **323**, 131 (2003).
[15] A. Goel, D.U. Tulyaganov, S. Agathopoulos, J.M.F. Ferreira, Ceram. Int. **34**, 505 (2008).
[16] M.J. Cattell, T.C. Chadwick, J.C. Knowles, R.L. Clarke, D.Y.D. Samarawickrama, Dental. Materials. **22,** 925 (2006).
[17] A. Goel, J.S. McCloy, K.M. Fox, C.J. Leslie, B.J. Riley, C.P. Rodriguez, M.J. Schweiger, J. Non-Cryst. Solids **358**, 674 (2012).
[18] E. Arroyabe, R. Tessadri, D.M. Tobbens, V. Kahlenberg, J. Am. Ceram. Soc. **94**, 2652 (2011).
[19] A.G. Kalampounias, N. K. Nasikas, G.N. Papatheodorou, J. Chem. Phys. **131**, 114513 (2009).
[20] K.N. Dalby, P.L. King, Am. Mineral. **91**, 1783 (2006).
[21] B.O. Mysen, D. Virgo, I. Kushiro, Am. Mineral. **66**, 678 (1981).
[22] P. Makreski, G. Jovanovski, B. Kaitner, J. Mol. Struct. **924–926**, 413 (2009).
[23] B. Reynard, J.D. Bass, J.M. Jackson, J. Eur. Ceram. Soc. **28**, 2459 (2008).
[24] M.C.Davis, K.J.Sanders, P.J.Grandinetti, S.J.Gaudio, S.Sen, J. Non-Cryst. Solids **357**, 2787 (2011).
[25] N. Seignez, A. Gauthier, D. Bulteel, M. Buatier, P. Recourt, D. Damidot, J.L. Potdevin, J. Hazard. Mater. **149**, 418 (2007).
[26] W.M.N. Nour, A.A. Mostafa, D.M. Ibrahim, Ceram. Int. 34, 101 (2008).
[27] L. Cormier, D.R. Neuville, Chem. Geol. **213**, 103 (2004).
[28] S. Sen, H. Maekawa, G.N. Papatheodorou, J. Phys. Chem. B **113**, 15243 (2009).
[29] K. Iishi, Am. Mineral. **63**, 1198 (1978).
[30] C-C. Lin, S-F. Chen, L-g. Liu, C-C. Li, Mat. Chem. Phys **123**, 569 (2010).
[31] P. Hudon, D.R. Baker, J. Non-Cryst. Solids **303**, 299 (2002).
[32] D. Boyd · M. R. Towler · R. V. Law · R. G. Hill**,** J. Mater. Sci.: Mater. Med. **17**, 397 (2006).

*Corresponding author: eanghel@hotmail.com